Monitoring Earth Surface Dynamics with Optical Imagery

Sébastien Leprince

Electrical Engineering
California Institute of Technology

May 16, 2008
Ph.D. Thesis Defense

Overview

- Objective: Monitoring natural phenomena involving Earth's surface dynamics, e.g., earthquakes, volcanoes, glacier flow, landslides, sand dunes migration, etc...

- Motivation: To validate/calibrate/refine physical models. To improve early evaluation of damage for large disasters

- Approach: Measuring horizontal ground deformations from optical satellite images: SPOT 1-2-3-4 (10 m), SPOT 5 (5 m and 2.5 m), ASTER (15 m), Quickbird (0.7 m), Aerial photographs (0.25-1 m)

Overview

- **Objective:** Monitoring natural phenomena involving Earth's surface dynamics, e.g., earthquakes, volcanoes, glacier flow, landslides, sand dunes migration, etc...

- **Motivation:** To validate/calibrate/refine physical models. To improve early evaluation of damage for large disasters

- **Approach:** Measuring horizontal ground deformations from optical satellite images: SPOT 1-2-3-4 (10 m), SPOT 5 (5 m and 2.5 m), ASTER (15 m), Quickbird (0.7 m), Aerial photographs (0.25-1 m)

Overview

- Objective: Monitoring natural phenomena involving Earth's surface dynamics, e.g., earthquakes, volcanoes, glacier flow, landslides, sand dunes migration, etc...
- Motivation: To validate/calibrate/refine physical models. To improve early evaluation of damage for large disasters
- Approach: Measuring horizontal ground deformations from optical satellite images: SPOT 1-2-3-4 (10 m), SPOT 5 (5 m and 2.5 m), ASTER (15 m), Quickbird (0.7 m), Aerial photographs (0.25-1 m)

Measuring deformation: a toy example

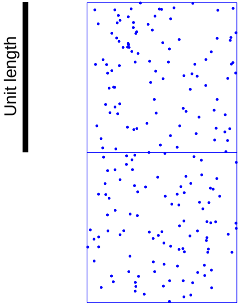

Measuring deformation: a toy example

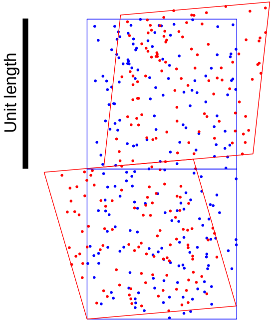

Measuring deformation: a toy example

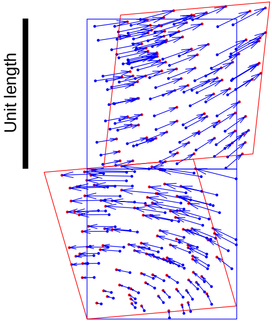

Measuring deformation: a toy example

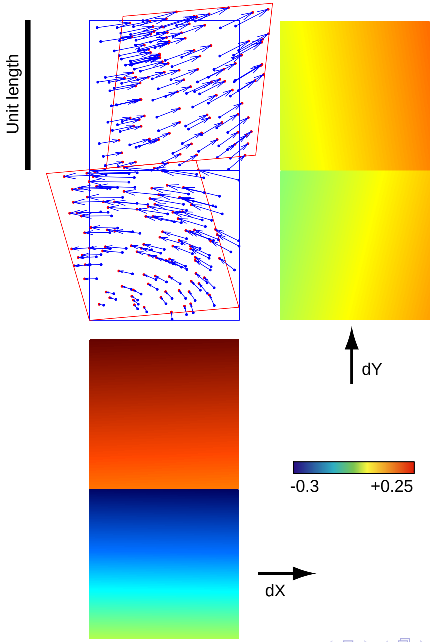

Measuring deformation: a toy example

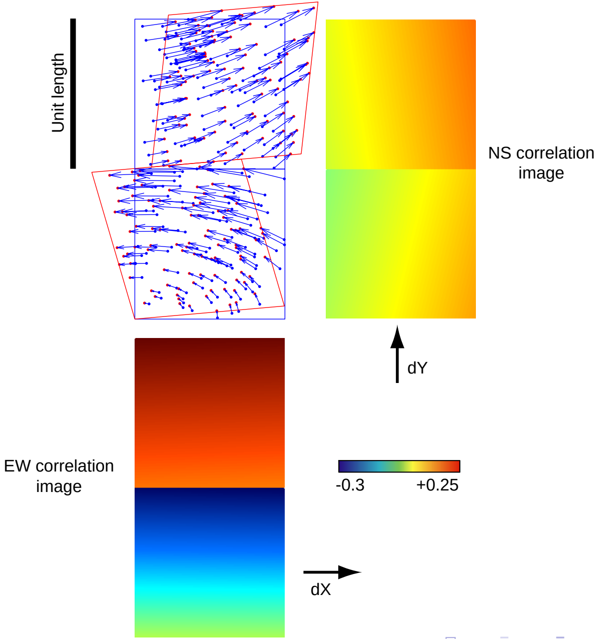

State of the Art, 2003: Hector Mine earthquake

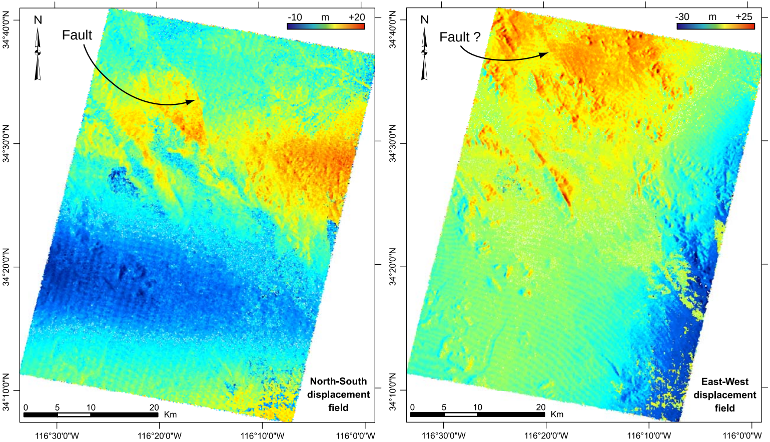

Do we see the fault discontinuity?

State of the Art, 2003: Hector Mine earthquake

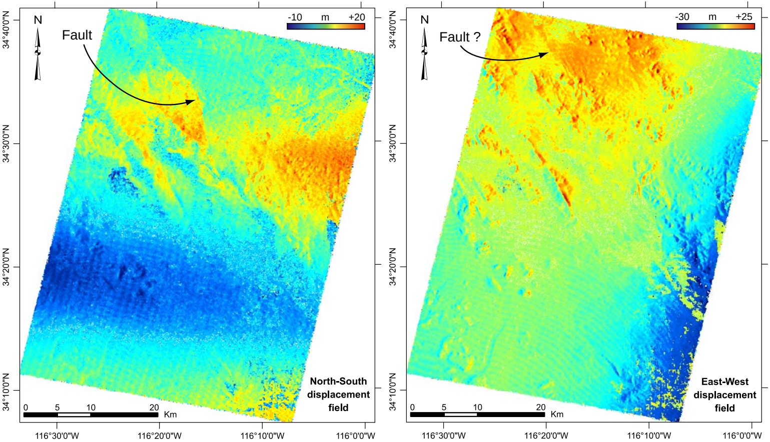

Pushbroom satellite: image lines depend on platform variations

State of the Art, 2003: Hector Mine earthquake

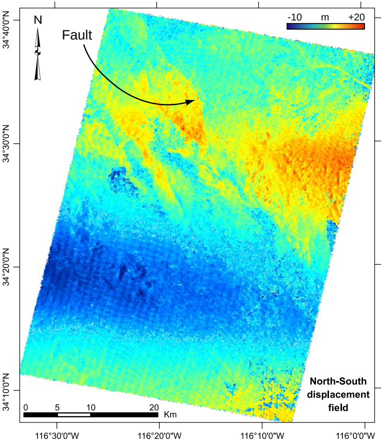

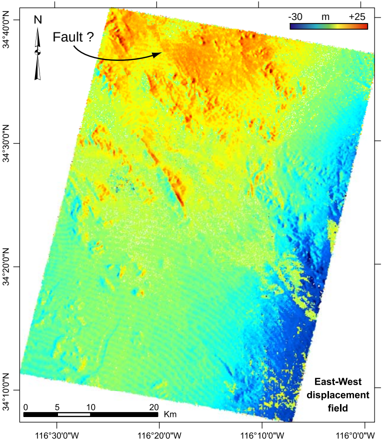

Topography artifacts due to stereoscopic parallax

State of the Art, 2003: Hector Mine earthquake

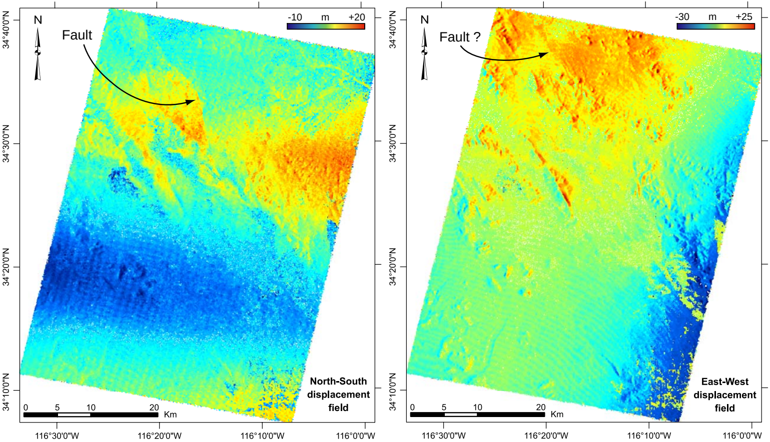

Parallax due to mis-registration and improper geometrical modeling

Lessons learned

- Viewing geometry of each pixel has to be physically modeled to account for topography and attitude variations
- Topography and images should be well registered
- Sub-pixel measurement accuracy required $\sim 1/20$ pixel size
- Images co-registration accuracy should be even smaller $\sim 1/50$ pixel size

Lessons learned

- Viewing geometry of each pixel has to be physically modeled to account for topography and attitude variations
- Topography and images should be well registered
- Sub-pixel measurement accuracy required $\sim 1/20$ pixel size
- Images co-registration accuracy should be even smaller $\sim 1/50$ pixel size

Lessons learned

- Viewing geometry of each pixel has to be physically modeled to account for topography and attitude variations
- Topography and images should be well registered
- Sub-pixel measurement accuracy required $\sim 1/20$ pixel size
- Images co-registration accuracy should be even smaller $\sim 1/50$ pixel size

Lessons learned

- Viewing geometry of each pixel has to be physically modeled to account for topography and attitude variations
- Topography and images should be well registered
- Sub-pixel measurement accuracy required $\sim 1/20$ pixel size
- Images co-registration accuracy should be even smaller $\sim 1/50$ pixel size

Measuring Horizontal Ground Displacement, Methodology Flow

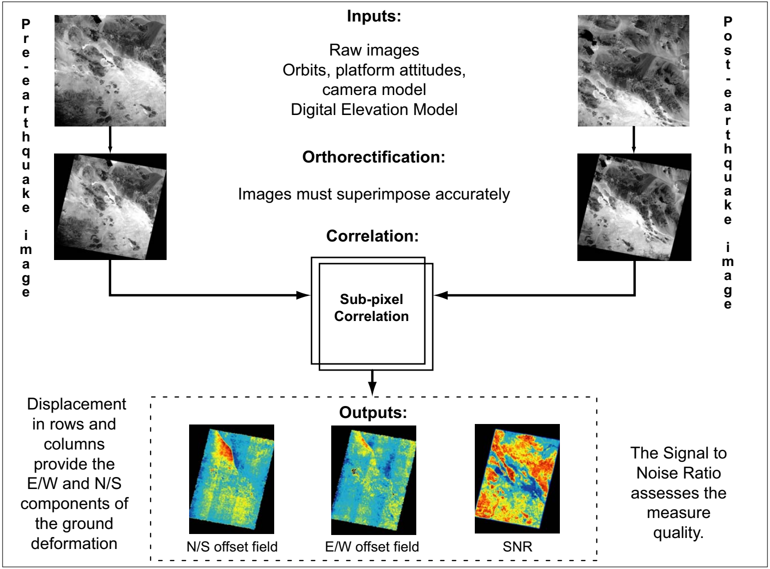

Orthoretification Model

Pushbroom acquisition geometry

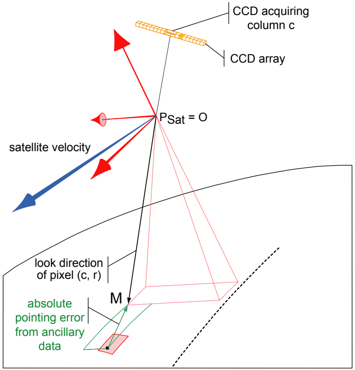

- O, optical center in space
- M, ground point seen by pixel p
- $\vec{u}_1$ pixel pointing model
- $R(p)$ 3D rotation matrix, roll, pitch, yaw at p
- $T(p)$ Terrestrial coordinates conversion
- $\vec{\delta}$ correction on the look directions to insure coregistration
- $\lambda > 0$

$$M(p) = O(p) + \lambda \left[T(p) R(p) \vec{u}_1(p) + \vec{\delta}(p) \right]$$

Orthorectification: An Irregular Mapping

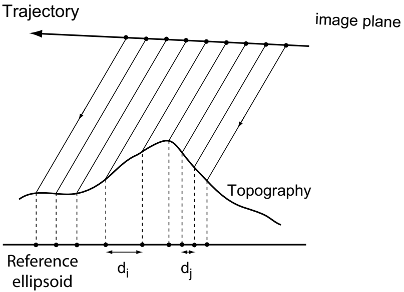

- Image pixels are assumed to regularly sample the image plane, but they sample the ground irregularly

Orthorectification: Inverse Model Principle

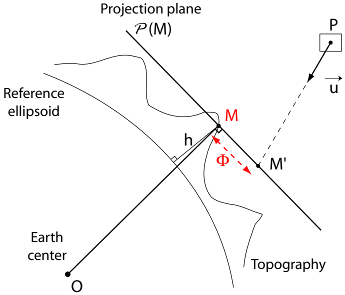

$$\Phi(x,y) = \|\overrightarrow{OM} - \overrightarrow{OM'}(x,y)\|^2$$

with

$$\overrightarrow{OM'}(x,y) = \overrightarrow{OP}(y) + \lambda^* \cdot \vec{u}(x,y)$$

and λ^* such that M' belongs to $\mathcal{P}(M)$

M given.

S. Leprince et al., IEEE TGRS, 2007

Orthorectification and Resampling

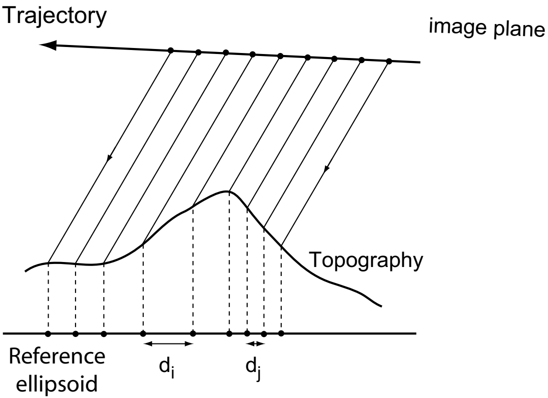

S. Leprince et al., IEEE TGRS, 2007

Orthorectification and Resampling

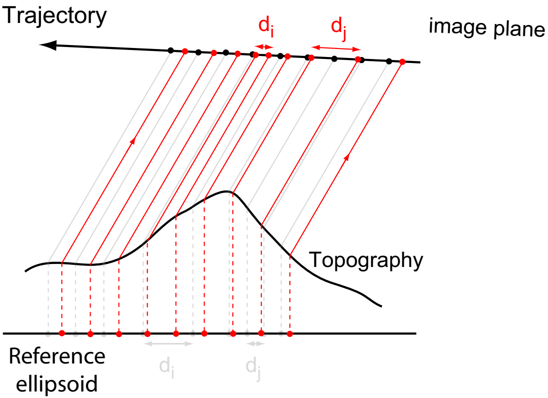

S. Leprince et al., IEEE TGRS, 2007

Orthorectification and Resampling

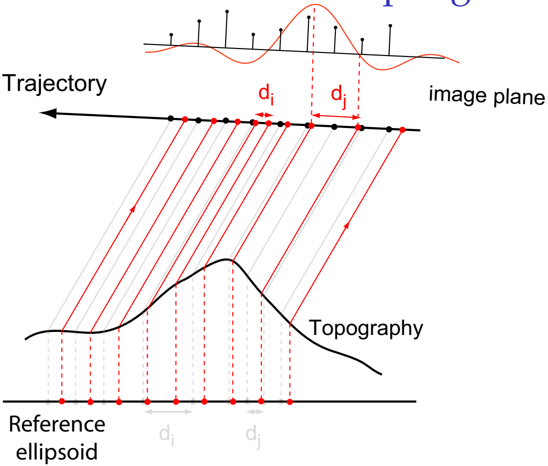

S. Leprince et al., IEEE TGRS, 2007

Orthorectification and Resampling

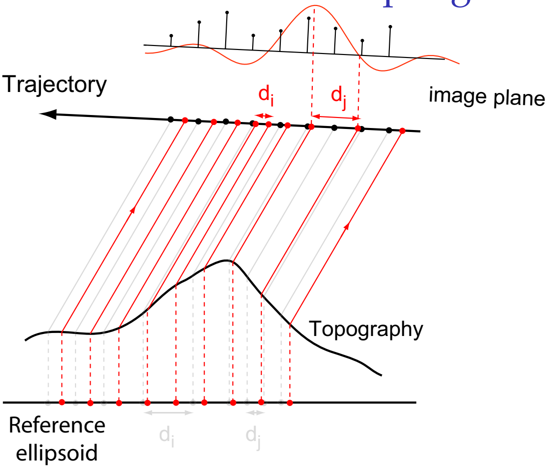

To avoid aliasing in the resampled signal, ideal resampling kernel:

$$h_d(x) = \frac{\sin \frac{\pi x}{d}}{\frac{\pi x}{d}}, \qquad \text{with } d = \max(1, \{d_i\})$$

S. Leprince et al., IEEE TGRS, 2007

Resampling

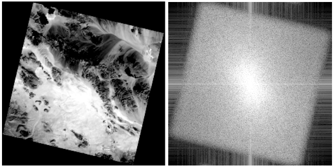

SPOT 10 m resolution, Rotation due to satellite orbit inclination. No aliasing, separability of the resampling kernel limits the sampling efficiency.

Resampling

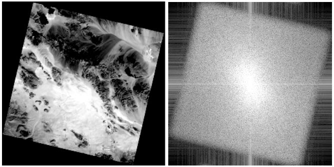

SPOT 10 m resolution, Rotation due to satellite orbit inclination. No aliasing, separability of the resampling kernel limits the sampling efficiency.

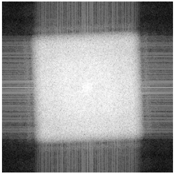

Aerial ortho-image spectrum
flat topography
1m resolution

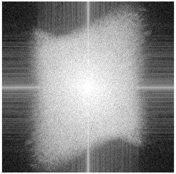

Aerial ortho-image spectrum
rough topography
1m resolution

Resampling distances increase/decrease with the topography gradient and the satellite incidence angle. Adaptive resampling distances would improve sampling efficiency.

Image Correlation: local rigid translations

- Fourier Shift Theorem

$$i_2(x,y) = i_1(x-\Delta_x, y-\Delta_y)$$
$$I_2(\omega_x,\omega_y) = I_1(\omega_x,\omega_y)e^{-j(\omega_x\Delta_x+\omega_y\Delta_y)}$$

- Normalized Cross-spectrum

$$C_{i_1i_2}(\omega_x,\omega_y) = \frac{I_1(\omega_x,\omega_y)I_2^*(\omega_x,\omega_y)}{|I_1(\omega_x,\omega_y)I_2^*(\omega_x,\omega_y)|} = e^{j(\omega_x\Delta_x+\omega_y\Delta_y)}$$

- Finding the relative displacement

$$\phi(\Delta_x,\Delta_y) = \sum_{\omega_x=-\pi}^{\pi}\sum_{\omega_y=-\pi}^{\pi} W(\omega_x,\omega_y)|C_{i_1i_2}(\omega_x,\omega_y) - e^{j(\omega_x\Delta_x+\omega_y\Delta_y)}|^2$$

W weighting matrix. (Δ_x,Δ_y) such that ϕ minimum.

S. Leprince et al., IEEE TGRS, 2007

Image Correlation: local rigid translations

- Fourier Shift Theorem

$$i_2(x,y) = i_1(x-\Delta_x, y-\Delta_y)$$
$$I_2(\omega_x,\omega_y) = I_1(\omega_x,\omega_y)e^{-j(\omega_x\Delta_x+\omega_y\Delta_y)}$$

- Normalized Cross-spectrum

$$C_{i_1 i_2}(\omega_x,\omega_y) = \frac{I_1(\omega_x,\omega_y)I_2^*(\omega_x,\omega_y)}{|I_1(\omega_x,\omega_y)I_2^*(\omega_x,\omega_y)|} = e^{j(\omega_x\Delta_x+\omega_y\Delta_y)}$$

- Finding the relative displacement

$$\phi(\Delta_x,\Delta_y) = \sum_{\omega_x=-\pi}^{\pi}\sum_{\omega_y=-\pi}^{\pi} W(\omega_x,\omega_y)|C_{i_1 i_2}(\omega_x,\omega_y) - e^{j(\omega_x\Delta_x+\omega_y\Delta_y)}|^2$$

W weighting matrix. (Δ_x,Δ_y) such that ϕ minimum.

S. Leprince et al., IEEE TGRS, 2007

Image Correlation: local rigid translations

- Fourier Shift Theorem

$$i_2(x,y) = i_1(x-\Delta_x, y-\Delta_y)$$
$$I_2(\omega_x,\omega_y) = I_1(\omega_x,\omega_y)e^{-j(\omega_x\Delta_x+\omega_y\Delta_y)}$$

- Normalized Cross-spectrum

$$C_{i_1i_2}(\omega_x,\omega_y) = \frac{I_1(\omega_x,\omega_y)I_2^*(\omega_x,\omega_y)}{|I_1(\omega_x,\omega_y)I_2^*(\omega_x,\omega_y)|} = e^{j(\omega_x\Delta_x+\omega_y\Delta_y)}$$

- Finding the relative displacement

$$\phi(\Delta_x,\Delta_y) = \sum_{\omega_x=-\pi}^{\pi}\sum_{\omega_y=-\pi}^{\pi} W(\omega_x,\omega_y)|C_{i_1i_2}(\omega_x,\omega_y) - e^{j(\omega_x\Delta_x+\omega_y\Delta_y)}|^2$$

W weighting matrix. (Δ_x,Δ_y) such that ϕ minimum.

S. Leprince et al., IEEE TGRS, 2007

Processing Chain

Select Image Registration Points from raw image

Process with manual input

Automatic process

S. Leprince et al., IEEE TGRS, 2007

Processing Chain

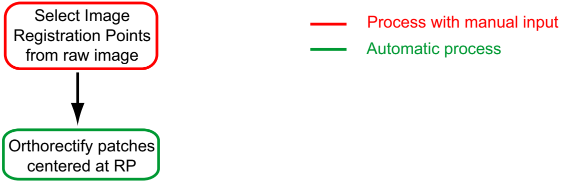

S. Leprince et al., IEEE TGRS, 2007

Processing Chain

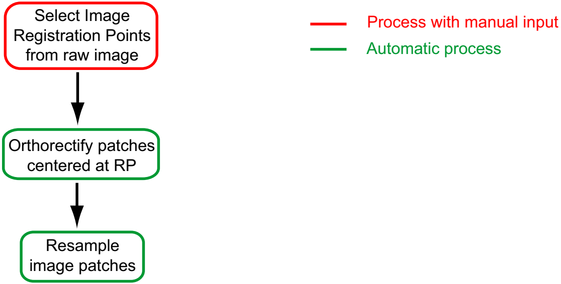

S. Leprince et al., IEEE TGRS, 2007

Processing Chain

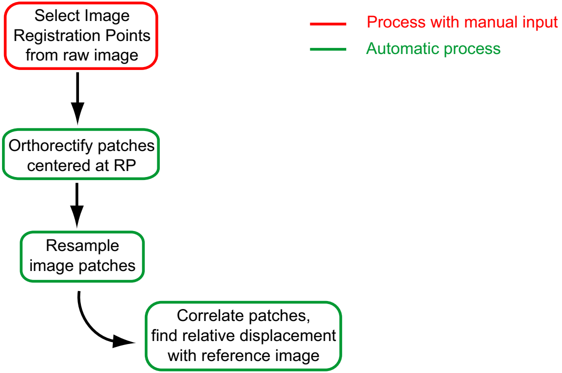

S. Leprince et al., IEEE TGRS, 2007

Processing Chain

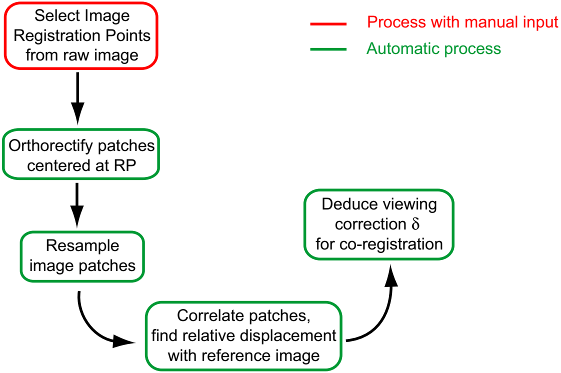

S. Leprince et al., IEEE TGRS, 2007

Processing Chain

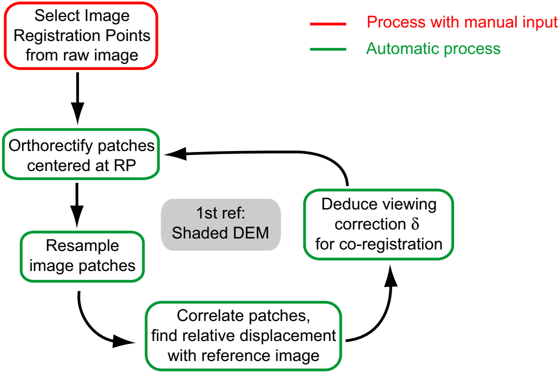

S. Leprince et al., IEEE TGRS, 2007

Processing Chain

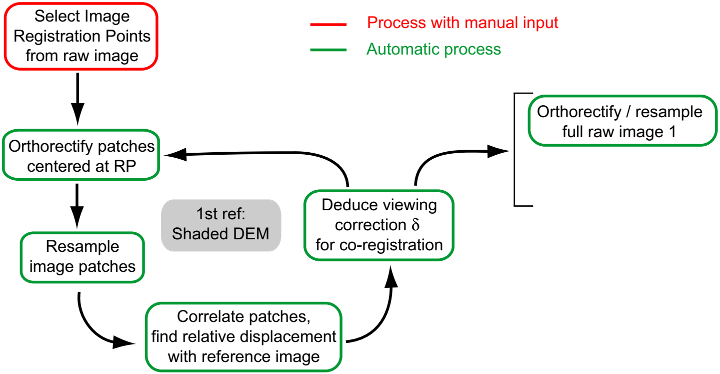

S. Leprince et al., IEEE TGRS, 2007

Processing Chain

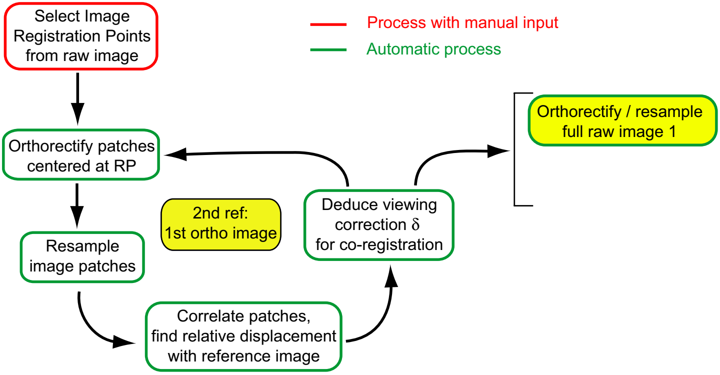

S. Leprince et al., IEEE TGRS, 2007

Processing Chain

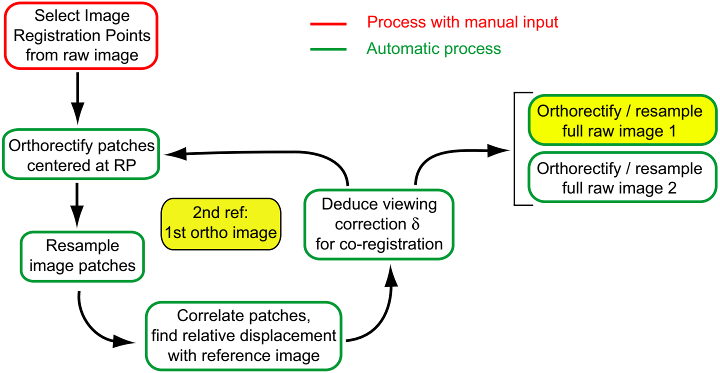

S. Leprince et al., IEEE TGRS, 2007

Processing Chain

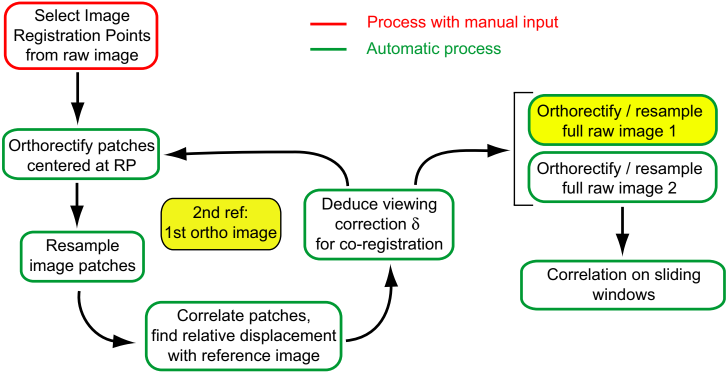

S. Leprince et al., IEEE TGRS, 2007

Processing Chain

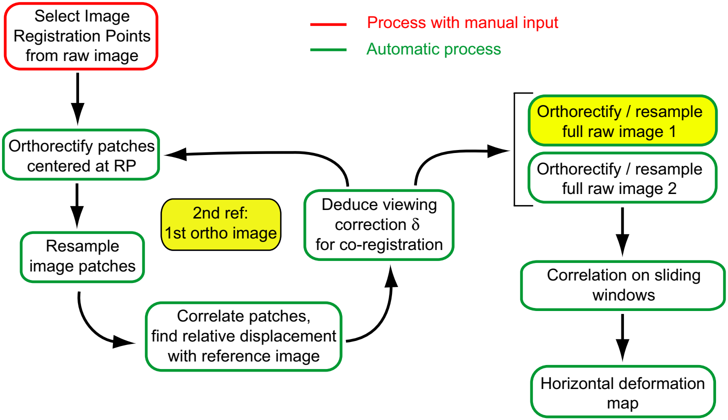

S. Leprince et al., IEEE TGRS, 2007

1999 Mw 7.1 Hector Mine Earthquake, CA

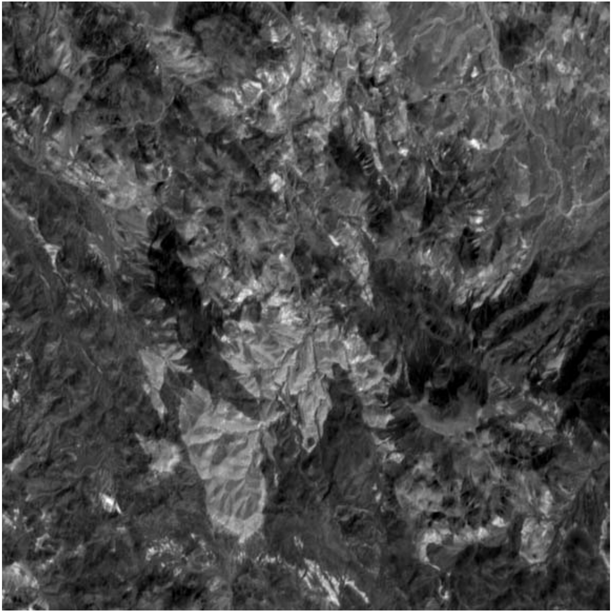

1999 Mw 7.1 Hector Mine Earthquake, CA

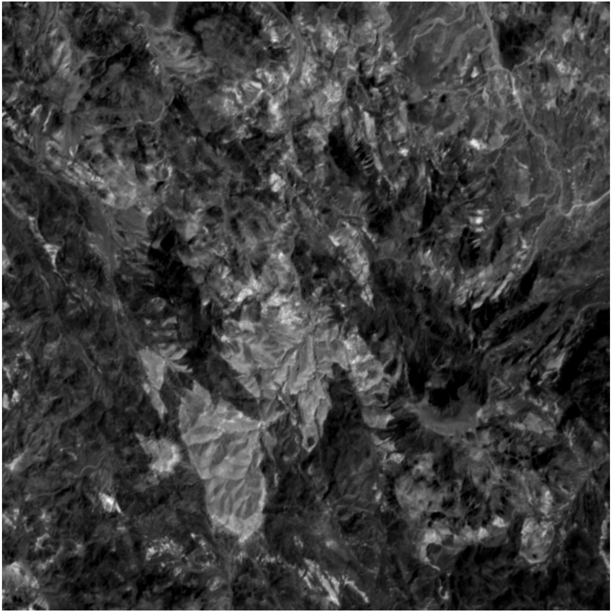

1999 Mw 7.1 Hector Mine Earthquake, CA

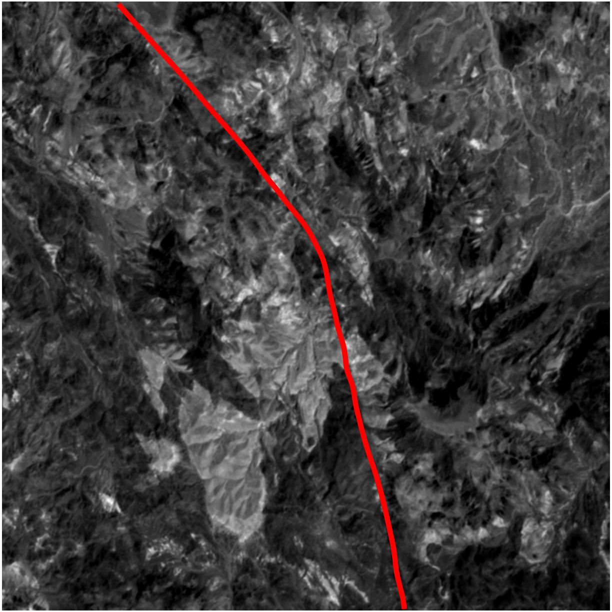

The 1999 Mw 7.1 Hector Mine Earthquake

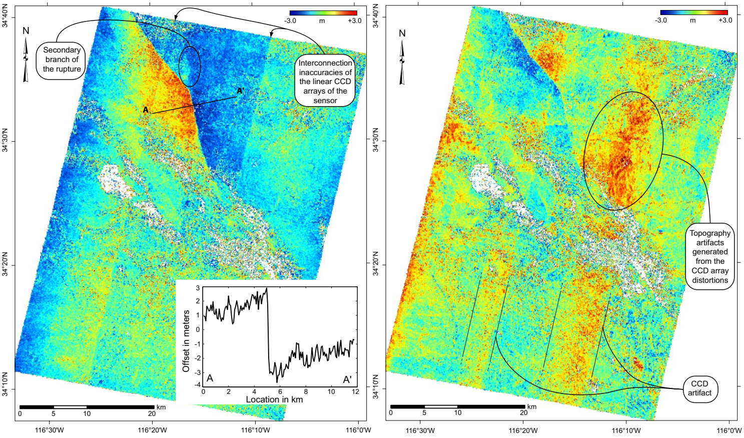

The Hector Mine horizontal coseismic field (NS and EW) from 10m SPOT4 1998 and 10m SPOT2 2000 images.

The 1999 Mw 7.1 Hector Mine Earthquake

SPOT CCD distortions

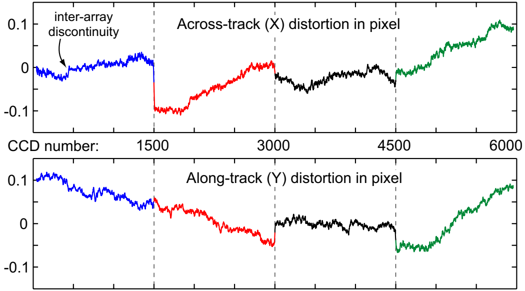

- Accurately calibrated (1/150 pixel) for SPOT 2/4 and accounted for in the orthorectification model

S. Leprince et al., IEEE TGRS, (in press) 2008

The 1999 Mw 7.1 Hector Mine Earthquake

SPOT CCD distortions

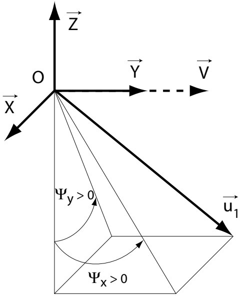

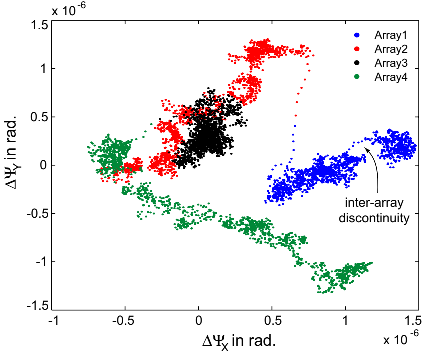

S. Leprince et al., IEEE TGRS, (in press) 2008

The 1999 Mw 7.1 Hector Mine Earthquake

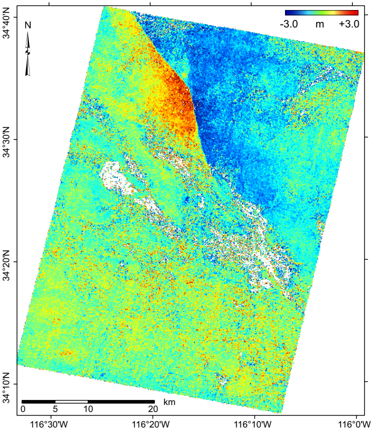

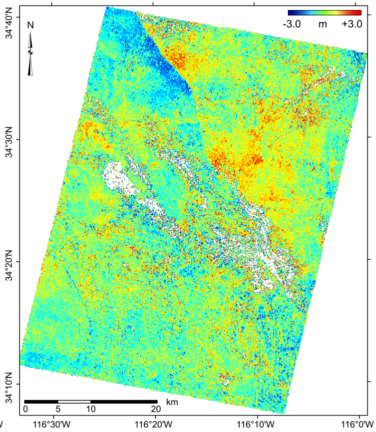

The Hector Mine horizontal coseismic field (NS and EW) once CCD distortions from SPOT4 and SPOT2 have been modeled during orthorectification

The 1999 Mw 7.1 Hector Mine Earthquake

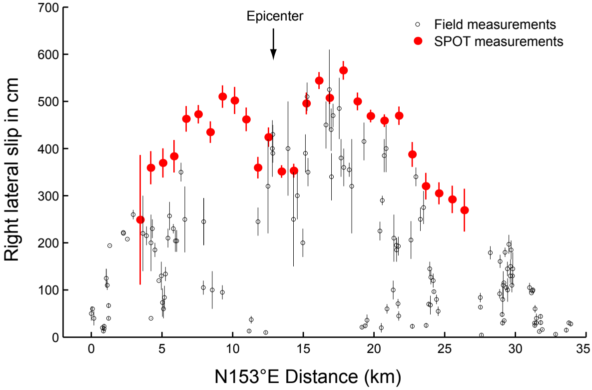

- Horizontal slip vectors measured from linear least square adjustment on each side of the fault. Perpendicular profiles are stacked over a width of 880 m and a length of 8 km.

Field measurements from J.A. Treiman et al., BSSA, 2002

The 1999 Mw 7.1 Hector Mine Earthquake

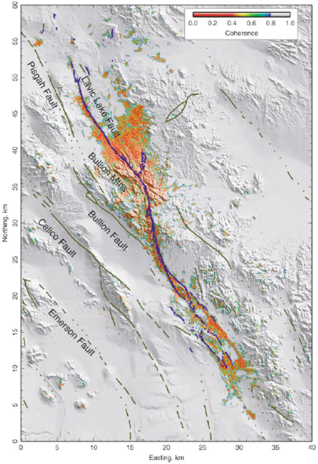

Figure 2. Interferometric coherence, C, for IP1, with $C > 0.8$ set to be transparent. Brown lines indicate known faults (Jennings, 1994). Surface rupture as observed in the field is indicated by the blue line (Treiman *et al.*, 2002). UTM zone 11 projection with origin at (116.457W 34.250N).

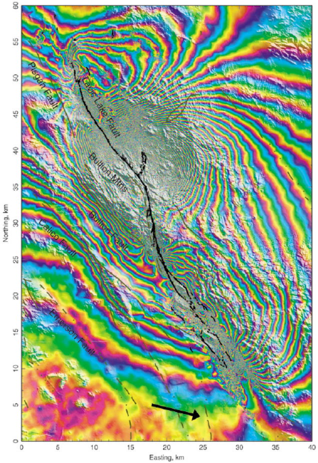

Figure 3. Same as Fig. 2 but color indicates wrapped phase for IP1. Each color cycle represents 2.8 cm of motion in the line-of-sight (LOS) direction. The black arrow represents the horizontal projection of the LOS vector toward the satellite.

M. Simons et al., BSSA, 2002

The 2005 Mw 7.6 Kashmir Earthquake

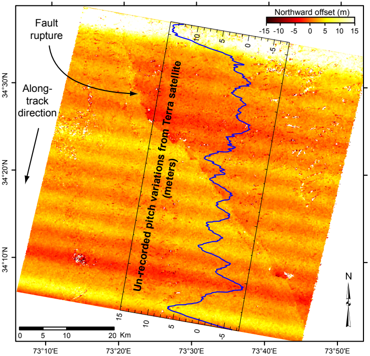

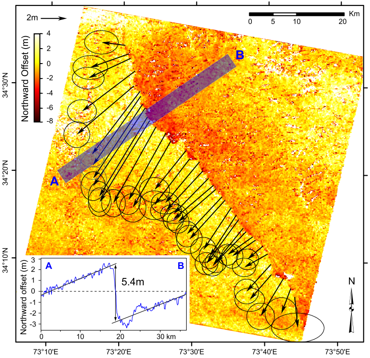

Northward component of the correlation from 15m ASTER images acquired on 11/14/2000 and 10/27/2005. Before, and after removing pitch artifacts (destripping). Deformation mostly perpendicular to the fault that could not be measured on the field

Leprince et al., IGARSS 2007 / Avouac et al., EPSL, 2006

The 2005 Mw 7.6 Kashmir Earthquake

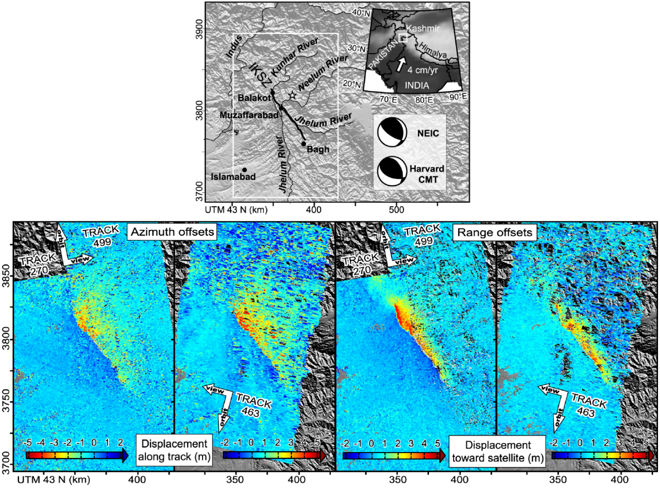

E. Pathier et al., GRL, 2006

The 2005 Mw 7.6 Kashmir Earthquake

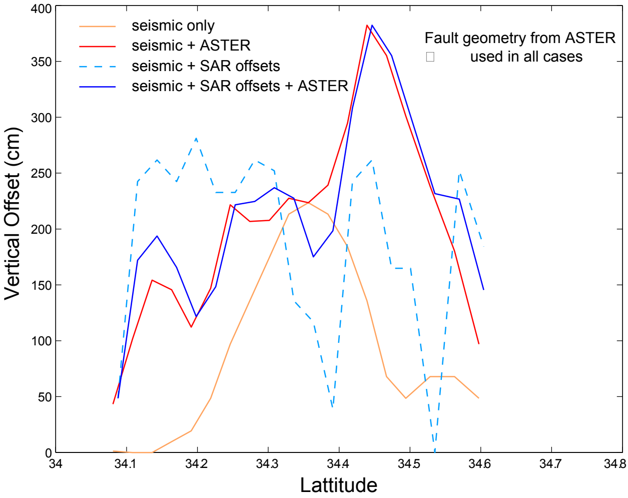

Collaboration A.O. Konca and D. Helmberger, Caltech

Aerial images: complementarity with satellite

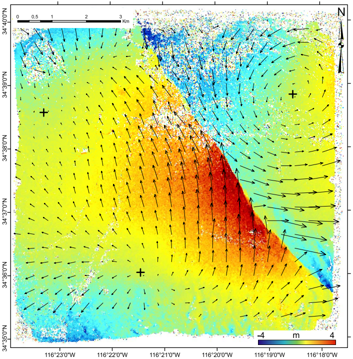

- Aerial photographs (1 m)
  USGS-NAPP
  7/25/89 - 06/01/02

- Introducing SPOT offsets allows to solve for longer deformation wavelength

Collaboration F. Ayoub, GPS, Caltech

Aerial images: complementarity with satellite

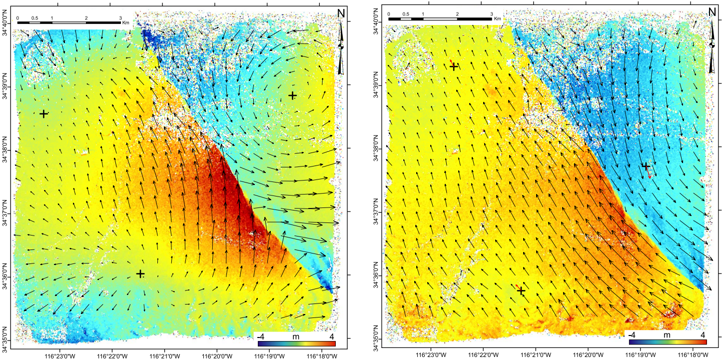

- Aerial photographs (1 m) USGS-NAPP 7/25/89 - 06/01/02
- Introducing SPOT offsets allows to solve for longer deformation wavelength

Collaboration F. Ayoub, GPS, Caltech

The 1992 Mw 7.3 Landers Earthquake, CA

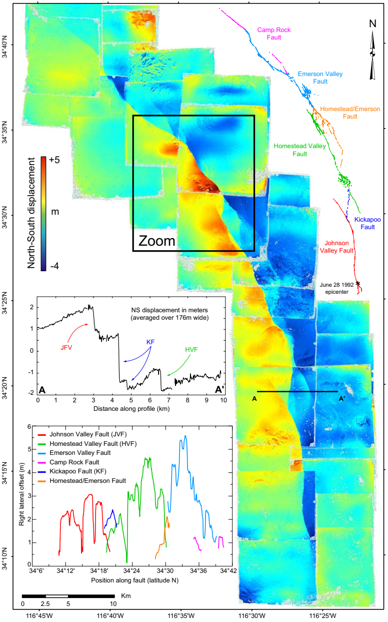

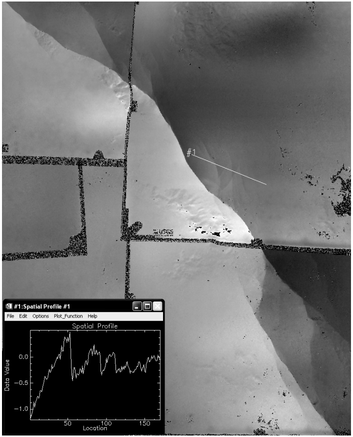

NS component - 30 pairs air photos from USGS - 1989-1995

SPOT5 used as reference

Collaboration F. Ayoub, Caltech, and Y. Klinger, IPG Paris, France

The Mer de Glace Glacier, France

SPOT 5 images
2.5 m resolution
2003-08-23
2003-09-18

The Mer de Glace Glacier, France

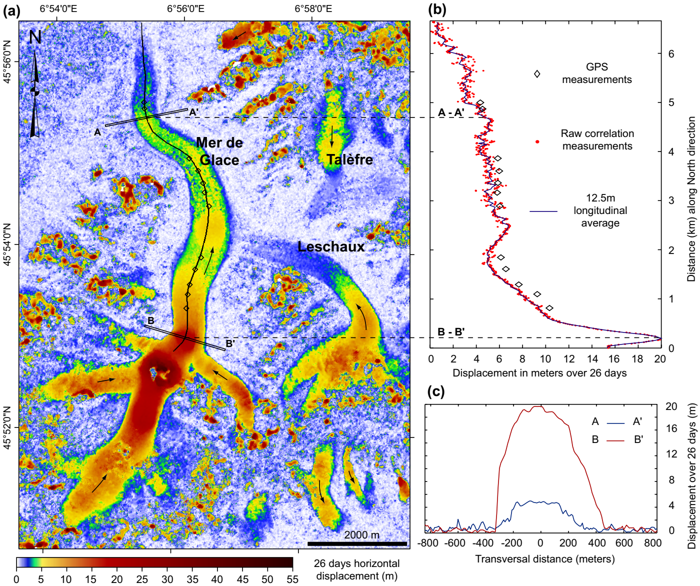

S. Leprince, et al., EOS, 2008

The La Valette Landslide, France

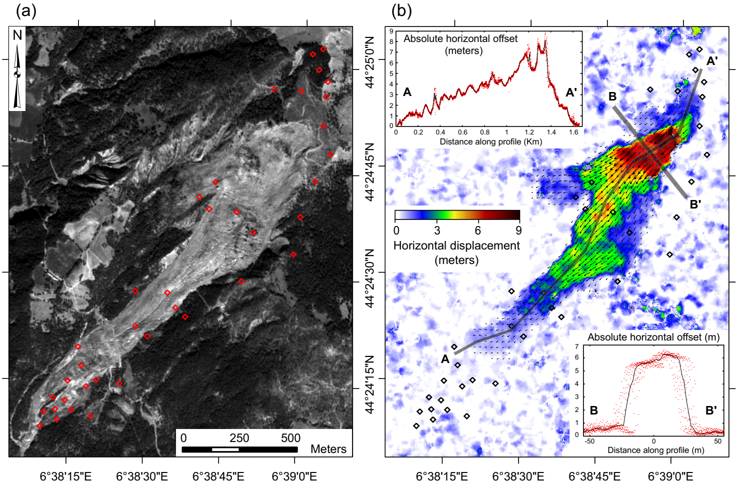

SPOT5 2.5m resolution images, 09/19/2003 - 08/22/2004

S. Leprince, et al., EOS, 2008

Conclusion: Technique limitations

- Resampling kernel
  - Separability implies oversampling depending on orbit inclination
  - Local resampling distances to avoid excess oversampling in flat terrain areas
- CCD distortions
  - Image plane not as regularly sampled as initially thought
  - Inverse model resampling challenged?
- Aliasing from Optics
  - Optical cut-off frequency $\approx$ 4-5 times CCD Nyquist frequency
  - Reduces the correlation accuracy by a factor > 10
  - Can bias the correlation under some conditions

Conclusion: Technique limitations

- Resampling kernel
  - Separability implies oversampling depending on orbit inclination
  - Local resampling distances to avoid excess oversampling in flat terrain areas
- CCD distortions
  - Image plane not as regularly sampled as initially thought
  - Inverse model resampling challenged?
- Aliasing from Optics
  - Optical cut-off frequency $\approx$ 4-5 times CCD Nyquist frequency
  - Reduces the correlation accuracy by a factor > 10
  - Can bias the correlation under some conditions

Conclusion: Technique limitations

- Resampling kernel
  - Separability implies oversampling depending on orbit inclination
  - Local resampling distances to avoid excess oversampling in flat terrain areas
- CCD distortions
  - Image plane not as regularly sampled as initially thought
  - Inverse model resampling challenged?
- Aliasing from Optics
  - Optical cut-off frequency $\approx$ 4-5 times CCD Nyquist frequency
  - Reduces the correlation accuracy by a factor > 10
  - Can bias the correlation under some conditions

Conclusion

- The technique has broad applications and is valuable to measure many different surface processes, e.g, glacier flow, landslides, sand dunes migration, volcanoes
- Complementary to InSAR that provides accurate measurement in the far field. Note that InSAR loses correlation when water content changes (pb with glaciers and landslides).
- Released an ENVI toolbox to make these algorithms available to the scientific community. COSI-Corr (Co-registration of Optically Sensed Images and Correlation) available for download since January 2007. COSI-Corr can process aerial photos, all SPOT (1,2,3,4,5) satellites, ASTER instrument, Quickbird satellite images, including all spectral bands.

Conclusion

- The technique has broad applications and is valuable to measure many different surface processes, e.g, glacier flow, landslides, sand dunes migration, volcanoes
- Complementary to InSAR that provides accurate measurement in the far field. Note that InSAR loses correlation when water content changes (pb with glaciers and landslides).
- Released an ENVI toolbox to make these algorithms available to the scientific community. COSI-Corr (Co-registration of Optically Sensed Images and Correlation) available for download since January 2007. COSI-Corr can process aerial photos, all SPOT (1,2,3,4,5) satellites, ASTER instrument, Quickbird satellite images, including all spectral bands.

Conclusion

- The technique has broad applications and is valuable to measure many different surface processes, e.g, glacier flow, landslides, sand dunes migration, volcanoes
- Complementary to InSAR that provides accurate measurement in the far field. Note that InSAR loses correlation when water content changes (pb with glaciers and landslides).
- Released an ENVI toolbox to make these algorithms available to the scientific community. COSI-Corr (Co-registration of Optically Sensed Images and Correlation) available for download since January 2007. COSI-Corr can process aerial photos, all SPOT (1,2,3,4,5) satellites, ASTER instrument, Quickbird satellite images, including all spectral bands.

Conclusion

Acknowledgments:

- Jean-Philippe Avouac (advisor), M. Simons, P. Perona, P.P. Vaidyanathan, and C. Elachi
- Francois Ayoub, Caltech, for the COSI-Corr code optimization and release
- Pablo Musé (Caltech), A.O. Konca (Caltech), E. Berthier (CNRS, France), Y. Klinger (IPGP, France), D. Scherler (Potsdam University, Germany), I. Barisin and B. Parsons (Oxford), C. Delacourt (IUEM, France), R. Michel and R. Binet (CEA, France), M. Taylor (KU), S. Barbot (UCSD)

The End: Thank you!

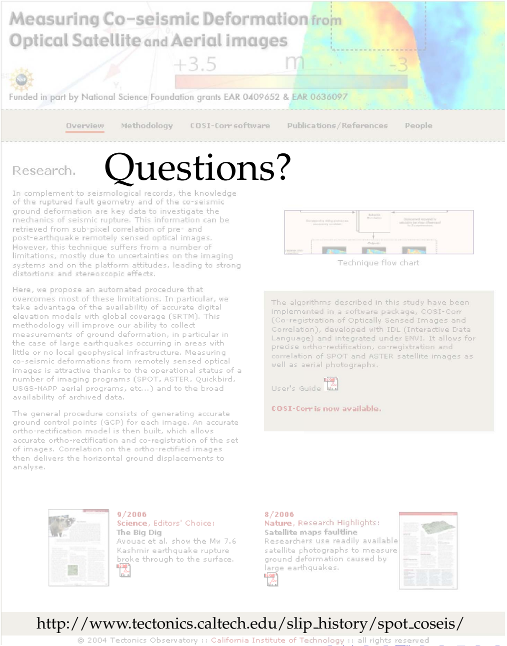
Measuring Co-seismic Deformation from Optical Satellite and Aerial images

+3.5 m -3

Funded in part by National Science Foundation grants EAR 0409652 & EAR 0636097

Overview Methodology COSI-Corr software Publications/References People

Research.

In complement to seismological records, the knowledge of the ruptured fault geometry and of the co-seismic ground deformation are key data to investigate the mechanics of seismic rupture. This information can be retrieved from sub-pixel correlation of pre- and post-earthquake remotely sensed optical images. However, this technique suffers from a number of limitations, mostly due to uncertainties on the imaging systems and on the platform attitudes, leading to strong distortions and stereoscopic effects.

Here, we propose an automated procedure that overcomes most of these limitations. In particular, we take advantage of the availability of accurate digital elevation models with global coverage (SRTM). This methodology will improve our ability to collect measurements of ground deformation, in particular in the case of large earthquakes occurring in areas with little or no local geophysical infrastructure. Measuring co-seismic deformations from remotely sensed optical images is attractive thanks to the operational status of a number of imaging programs (SPOT, ASTER, Quickbird, USGS-NAPP aerial programs, etc...) and to the broad availability of archived data.

The general procedure consists of generating accurate ground control points (GCP) for each image. An accurate ortho-rectification model is then built, which allows accurate ortho-rectification and co-registration of the set of images. Correlation on the ortho-rectified images then delivers the horizontal ground displacements to analyse.

Technique flow chart

The algorithms described in this study have been implemented in a software package, COSI-Corr (Co-registration of Optically Sensed Images and Correlation), developed with IDL (Interactive Data Language) and integrated under ENVI. It allows for precise ortho-rectification, co-registration and correlation of SPOT and ASTER satellite images as well as aerial photographs.

User's Guide

COSI-Corr is now available.

9/2006
Science, Editors' Choice:
The Big Dig
Avouac et al. show the Mw 7.6 Kashmir earthquake rupture broke through to the surface.

8/2006
Nature, Research Highlights:
Satellite maps faultline
Researchers use readily available satellite photographs to measure ground deformation caused by large earthquakes.

Questions?

http://www.tectonics.caltech.edu/slip_history/spot_coseis/

COSI-Corr web site

SPOT images

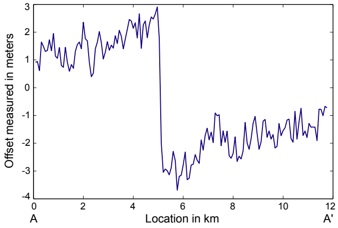

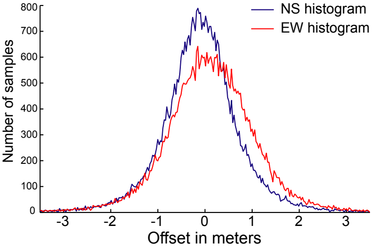

Profile AA′ from NS correlation image. Maximum displacement of 6 m in the NS direction. High frequency noise accounts for about 80-85 cm.

- Typical offset uncertainty on a single profile $\sigma \approx 30$ cm

- μ_{NS} = -7.4 cm $\sigma_{NS} = 82$ cm
- $\mu_{EW} = 18.3$ cm $\sigma_{EW} = 92$ cm
- Average mis-registration 20 cm $\approx \frac{1}{50}$ of the pixel size

Resampling: irregularly spaced data

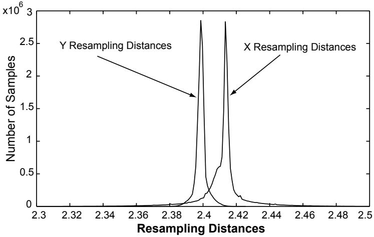

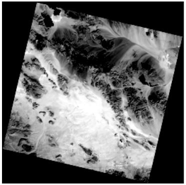

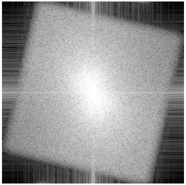

- Resampling of a SPOT 5 image, 5 m nominal ground resolution, on a 10 m grid. Jittered sampling verified.
- No aliasing. ≈ 12.5 m effective resolution due to satellite orbit inclination. Oversampling due to separable kernel

Resampling: limitations

- Separability of the resampling kernel limits the sampling efficiency: a more efficient kernel would be rotated along the satellite track
- Resampling distances increase/decrease with the topography gradient and the satellite incidence angle. Considering the worst case over the whole image may lead to increased low pass filtering on parts of the image where the topography is flat. Effect more pronounced as the image resolution increases. Adaptive resampling distances.

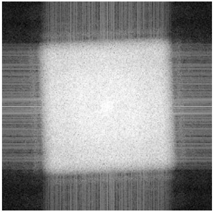

Aerial ortho-image spectrum
flat topography
1m resolution

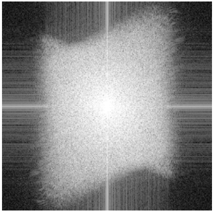

Aerial ortho-image spectrum
rough topography
1m resolution

Resampling: regularly spaced data

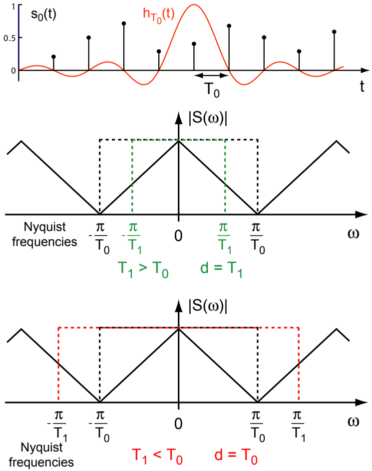

$s_0(t)$ bandlimited at Nyquist frequency $\frac{\pi}{T_0}$, to be resampled at a new sampling period T_1

Ideal resampling kernel:

$$h_d(t) = \frac{\sin \frac{\pi t}{d}}{\frac{\pi t}{d}}$$

To avoid aliasing in the resampled signal:

- $d = \max(T_0, T_1)$

d effective signal "resolution"

Resampling: irregularly spaced data

Application to 2D inverse mapping

- 2D separable sinc kernel

$$h_{d_x,d_y}(x,y) = \frac{\sin \frac{\pi x}{d_x}}{\frac{\pi x}{d_x}} \cdot \frac{\sin \frac{\pi y}{d_y}}{\frac{\pi y}{d_y}}$$

- $\{d_{x_0}\} = \{d_{y_0}\} = \{1\}$ raw image regularly sampled every pixel
- $d_x = \max(1, \{d_{x_1}\})$ and $d_y = \max(1, \{d_{y_1}\})$
- $\{d_{x_1}\}$ and $\{d_{y_1}\}$ determined from local absolute differences in ground pixel projections
- Images slightly low-pass filtered, but not a limitation under the assumption of jittered sampling

Correlation: function to minimize

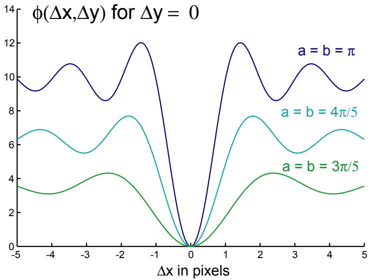

- Worst case for initialization accuracy ± 1 pixel. Can be achieved with the peak correlation method.
- Minimization with a gradient descent algorithm

Frequency Masking

- To remove resampling cut off frequencies
- To give less confidence where the signal as low energy
- To lower sensitivity to aliasing from optics

Correlation: Synthetic Example

Quality of the correlation on 3000 × 3000 pixels images. A shifted image is made from sinc resampling. 32 × 32 pixels correlation windows scan the test images with a step of 16 pixels. 32400 correlation measures are gathered on each test.

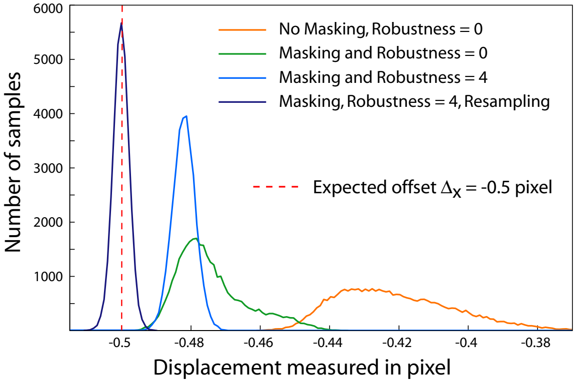

- $\mu = -0.42 \ \sigma = 0.017$
- $\mu = -0.47 \ \sigma = 0.010$
- $\mu = -0.48 \ \sigma = 0.003$
- $\mu = -0.498 \ \sigma = 0.002$

Technique limitation:

Aliasing

- Optical cut-off frequency ≈ 4-5 times the CCD Nyquist frequency on SPOT 1-4
- Can be formalized as a super-resolution pb for the correlation
- Aliasing could be avoided by defocusing of proper adjustment of the bias voltage in back illuminated CCD (would required deconvolution to recover sharp image)

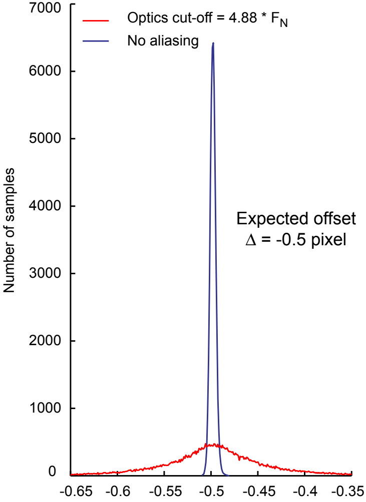

- $\mu_{noalias}$ = - 0.498 $\sigma_{noalias}$ = 0.002
- μ_{alias} = - 0.496 σ_{alias} = 0.07

The AFAR rift in Ethiopia, 2005 events

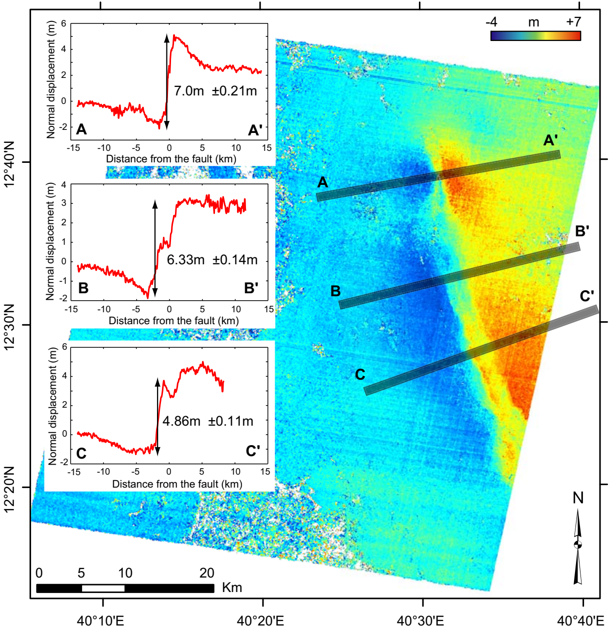

EW displacement field, from 10m SPOT 4 images, 12/19/2004 01/13/2006

Collaboration I. Barisin and B. Parsons, University of Oxford, UK

The 1999 Mw 7.4 Izmit and Mw 7.2 Duzce Earthquakes

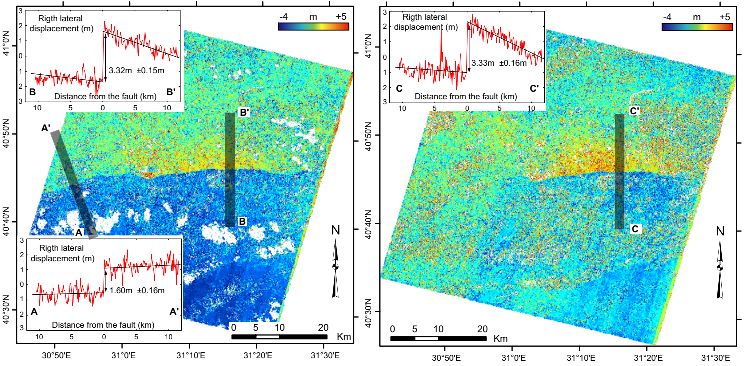

EW component of displacement field, from 10m SPOT images acquired on 21/06/1999, 03/10/1999, and 12/07/2000

Collaboration A.O. Konca and D. Helmberger, Caltech

The Great Sand Dunes, Colorado

The Great Sand Dunes, Colorado

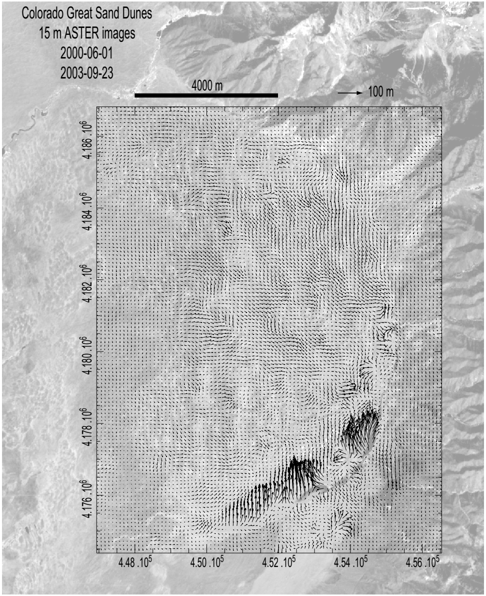

Sand Dunes Migration, Morocco

Laayoun, Maroc

ASTER images acquired in 2001 and 2006

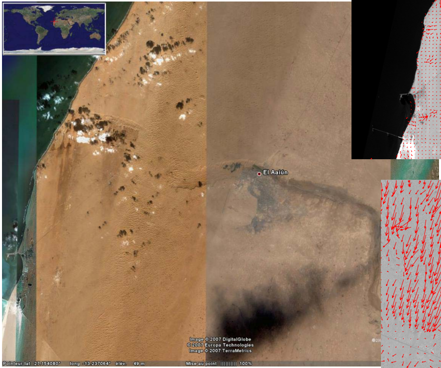

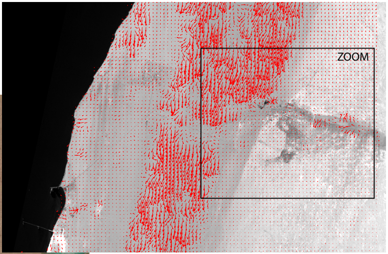

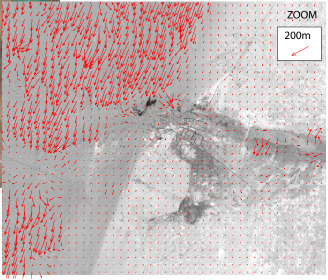

Collaboration, Mohamed Chlieh, IRD, France